The Journal of Neuroscience, July 1, 1999, *19*(13):5255–5264

Molecular Basis for the Inactivation of Ca^{2+}- and Voltage-Dependent BK Channels in Adrenal Chromaffin Cells and Rat Insulinoma Tumor Cells

Xiao-Ming Xia,[1] Jiu Ping Ding,[1] and Christopher J. Lingle[1,2]

Departments of [1]Anesthesiology and [2]Anatomy and Neurobiology, Washington University School of Medicine, St. Louis, Missouri 63110

Large-conductance Ca^{2+}- and voltage-dependent potassium (BK) channels exhibit functional diversity not explained by known splice variants of the single *Slo* α-subunit. Here we describe an accessory subunit (β3) with homology to other β-subunits of BK channels that confers inactivation when it is coexpressed with *Slo*. Message encoding the β3 subunit is found in rat insulinoma tumor (RINm5f) cells and adrenal chromaffin cells, both of which express inactivating BK channels. Channels resulting from coexpression of *Slo* α and β3 subunits exhibit properties characteristic of native inactivating BK channels. Inactivation involves multiple cytosolic, trypsin-sensitive domains. The time constant of inactivation reaches a limiting value ~25–30 msec at Ca^{2+} of 10 μM and positive activation potentials. Unlike *Shaker* N-terminal inactivation, but like native inactivating BK channels, a cytosolic channel blocker does not compete with the native inactivation process. Finally, the β3 subunit confers a reduced sensitivity to charybdotoxin, as seen with native inactivating BK channels. Inactivation arises from the N terminal of the β3 subunit. Removal of the β3 N terminal (33 amino acids) abolishes inactivation, whereas the addition of the β3 N terminal onto the β1 subunit confers inactivation. The β3 subunit shares with the β1 subunit an ability to shift the range of voltages over which channels are activated at a given Ca^{2+}. Thus, the β-subunit family of BK channels regulates a number of critical aspects of BK channel phenotype, including inactivation and apparent Ca^{2+} sensitivity.

Key words: accessory subunits; K^+ channels; BK channels; Ca^{2+}- and voltage-gated K^+ channels; mSlo channels; inactivation

Large-conductance calcium (Ca^{2+}) and voltage-gated K^+ channels are widely expressed channels (McManus, 1991) that couple changes in submembrane Ca^{2+} concentration ($[Ca^{2+}]_i$) to the regulation of electrical excitability. BK channels are formed from four α-subunits (Shen et al., 1994) arising from the *Slo* gene product (Atkinson et al., 1991; Adelman et al., 1992; Butler et al., 1993). In addition, in some tissues, including smooth muscle (Knaus et al., 1994a,b) and cochlea (Ramanathan et al., 1999), an accessory β-subunit can regulate BK channel gating profoundly. β-Subunits appear to be responsible for the increased sensitivity of smooth muscle BK channels to Ca^{2+} (McManus et al., 1995) and may play a role in the frequency tuning of hair cells (Ramanathan et al., 1999). Although β-subunits may account for some of the diversity of BK channels, the BK phenotype in many cells remains unexplained (McManus, 1991). For example, in adrenal chromaffin cells (Solaro and Lingle, 1992), pancreatic β-cell lines (Li et al., 1999), and in the hippocampus (Hicks and Marrion, 1998) some BK channels exhibit inactivation. Furthermore, in *Drosophila* flight muscles (Salkoff, 1983) and perhaps in hair cells (Armstrong and Roberts, 1999), there are inactivating Ca^{2+}-dependent currents probably arising from the *Slo* gene product. Thus, under conditions of sustained $[Ca^{2+}]_i$ and depolarization, such BK-type channels initially activate and then become silent. The inactivation of BK channels may play a role in the regulation of electrical excitability in these cells by altering the availability of BK channels for rapid repolarization after an action potential.

The most studied form of inactivation of BK channels has been in rat adrenal chromaffin cells (Solaro and Lingle, 1992; Solaro et al., 1995, 1997; Ding et al., 1998). The inactivation of chromaffin cell BK channels (BK_i channels) shares some features with N-terminal type inactivation of voltage-dependent K^+ channels (Hoshi et al., 1990). As with the *Shaker*B channel (Hoshi et al., 1990; Gomez-Lagunas and Armstrong, 1995), BK_i inactivation arises from multiple trypsin-sensitive cytosolic domains (Ding et al., 1998). However, in contrast to the open channel-like blockade produced by the *Shaker*B N-terminal peptide (Choi et al., 1991; Demo and Yellen, 1991), cytosolic blockers of the BK channel pore do not compete with the native inactivation domain (Solaro et al., 1997). Previous work has failed to reveal a *Slo* α-subunit splice variant that might account for the inactivating phenotype (Saito et al., 1997).

Here we describe an EST sequence that encodes a homolog of the previously identified BK β-subunits [β1, Knaus et al. (1994a); β2, Oberst et al. (1997)]. This new subunit (β3) confers inactivation on BK channels, and message-encoding β3 is found in both chromaffin cells and rat insulinoma tumor (RINm5F) cells. We also show that, in terms of inactivation rates, dependency on voltage and Ca^{2+}, lack of effect of cytosolic blockers, sensitivity to trypsin, and relative insensitivity to charybdotoxin (CTX), the channels arising from the coexpression of *Slo* and β3 subunits

Received Feb. 25, 1999; revised April 9, 1999; accepted April 14, 1999.

This work was supported by National Institutes of Health Grant DK46564 to C.L. We thank Dr. Graeme Bell for providing the RINm5f cDNA library, Vani Kalyanaraman for technical assistance, and Anne Benz and Chuck Zorumski for providing us with oocytes.

Correspondence should be addressed to Dr. Chris Lingle, Department of Anesthesiology, Washington University School of Medicine, Box 8054, 660 South Euclid Avenue, St. Louis, MO 63110.

share key properties with native BK_i channels in chromaffin cells and RIN cells.

MATERIALS AND METHODS

Isolation of cDNA clones. A novel member of the BK β-subunit family, β3, was identified in the human EST database on the basis of homology with the known human β1 (Knaus et al., 1994b) and quail β2 (Oberst et al., 1997) subunits. The EST clone (accession number AA904191) containing the human β3 cDNA (accession number pending) then was obtained from a human lung neuroendocrine tumor library (Genome Systems, St. Louis, MO). The rat β3 homolog (accession number pending) was isolated from a RINm5F cDNA library (gift of Dr. Graeme Bell, University of Chicago, IL). The hybridization was performed in 1 M NaCl, 1% SDS, and 50% formamide at 37°C overnight and then washed with 2× SSC and 0.5% SDS. The screening membranes were exposed to x-ray film for 2 d. Initially, eight positive clones were identified in the RINm5F library. Of these, two purified positive cDNA clones contained full-length coding sequences of 1360 and 1042 bp, respectively. The DNA sequencing was performed with a BigDye Terminator Sequencing Kit (Applied Biosystems, Foster City, CA) on both strands. The β-clones were all subcloned into pBF vector for *in vitro* RNA synthesis (Xia et al., 1998b).

Tissue distribution of BK β3 subunits. Northern blots were performed on membranes obtained from Clontech (Palo Alto, CA). Northern blots contained ~2 μg of poly(A^+) RNA per lane from the indicated tissues. The loading of each lane was adjusted to contain an equal amount of human β-actin per lane, based on a previous blot that used human β-actin cDNA as a probe. The experimental procedure was as previously described (Xia et al., 1998a). Expression of rβ3 in adrenal and pancreatic tissue was determined by PCR and confirmed by sequence analysis. Total RNA from adrenal and pancreas was extracted and reversed-transcribed to cDNA (Promega, Madison, WI). Two primers (5′ rβ3 5′-ACCATGACCTCCTGGACAAAAGG-3′ and 3′ rβ3 5′-TTCTGTG-TGGTAGAGGAGGAGCT-3′) were used for the PCR reaction (*Taq* polymerase, 32 cycles: 94°C for 30 sec, 52°C for 30 sec, and 72°C for 30 sec). Then the PCR products were subjected to automatic sequencing.

Expression constructs. The *mSlo* α-subunit (accession number L16912; Butler et al., 1993) used in these experiments was identical to that used in previous work from this lab (mbr5; Wei et al., 1994; Saito et al., 1997). Specifically, we used a construct containing no insert at the mammalian splice site 2 (Tseng-Crank et al., 1994). RNA from rat adrenal chromaffin cells also contains other splice site 2 variants (Saito et al., 1997), including a 59 or 61 amino acid insert (Saito et al., 1997; Xie and McCobb, 1998; Li et al., 1999). The longer forms confer an ~20 mV leftward shift in the voltage dependence of gating at a given Ca^{2+}. In preliminary experiments in which the β3 subunit was coexpressed with the *Slo* construct containing the 59 amino acid insert, the resulting channels exhibited inactivation. The *mSlo* construct was subcloned in pBScMXT.

To make the hβ1 construct for expression, we used two hβ1 specific oligonucleotides each with a *Xba*I or *Sal*I tail (5′-ACTATCTAG-ACCCAGTGAATATGGTGAAGAAGCT-3′ and 5′-TACTAGTCG-ACTGGCTCTACTTCTGGGCCGC-3′) in a PCR reaction (pfu polymerase, Stratagene), using hβ1 (accession number U38907; the generous gift of the Merck Research Labs, West Point, PA) as the DNA template. Then the product was digested and subcloned in pBF vector (Xia et al., 1998b).

The N-terminal deletion [hβ3(Δ1–33)] construct also was produced via PCR reaction (5′-GGAATTCTCTAAGATGAGGAAAACAGT-CACAGCAC-3′ and 5′-TACTAGTCGACAAAAATTATTTTATC-CATTTTTG-3′) and subcloned in pBF. To generate C43A189 [hβ3(1–43): hβ1], we applied two rounds of PCR. In the first-round PCR, reaction A used hβ1 as the DNA template with two primers: one was a specific primer of 3′ hβ1 (5′-TACTAGTCGACTGGCTCTACTTCTGGGCCGC-3′), and the second one was a bipartisan primer of sense strand of hβ3 and hβ1 (5′-ACAGCACTGAAGGCAGGAGAGACACGAGCCCTTTG-3′). Reaction B used hβ3 as a template with two primers: one was a specific primer of 5′ hβ3 (5′-AAGGAATCTAGACCCTGGACCAACATTCTCTAAG-3′), and the other one was another bipartisan primer of antisense of hβ1 and hβ3 (5′-CAAAGGGCTCGTGTCTCTCCTGCCTTCAGTGCTGT-3′). This latter primer is the complement of the previous bipartisan primer (pfu polymerase, 32 cycles, 96°C for 30 sec, 51°C for 45 sec, and 72°C for 1 min). In the second-round PCR, the products of first-round PCR were used as a template (equal volume mixture of reaction A and B), and the two specific primers of hβ1 and hβ3 (5′ hβ3 primer and 3′ hβ3 primer) were used as primers (pfu polymerase, 32 cycles, 96°C for 30 sec, 51°C for 45 sec, and 72°C for 1.5 min) (Tucker et al., 1996). Then the final product was digested with *Xba*I and *Sal*I and subcloned in pBF. All of the constructs were verified by DNA sequencing.

Expression in Xenopus *oocytes. In vitro* transcription was performed to prepare ^{M7}GppGp-capped cRNA for oocyte injection. First the plasmids were linearized with an appropriate enzyme (*Sal*I for *mSlo* and *Mlu*I for β-constructs). T3 (*mSlo* construct; Wei et al., 1994) or Sp6 (all β-related constructs) RNA polymerases were used for run-off transcription (Xia et al., 1998b). Total cRNA (0.1–0.5 ng) was injected into stage IV *Xenopus* oocytes that were harvested the day before. By weight, the ratio of α- to β-subunit RNA was 1:1 or 1:2, ensuring a large molar excess of β-subunit RNA.

Electrophysiological recordings were performed after 1–7 d incubation of oocytes in ND-96 [containing (in mM) 96 NaCl, 2.0 KCl, 1.8 $CaCl_2$, 1.0 $MgCl_2$, and 5.0 HEPES, pH 7.5] supplemented with sodium pyruvate (2.5 mM), penicillin (100 U/ml), streptomycin (100 μg/ml), and gentamicin (50 μg/ml).

Electrophysiology. Currents were recorded in either inside-out or outside-out patches (Hamill et al., 1981). The generation of ensemble averages of detected channel openings (1–10 channels in patch) was done with patches from oocytes maintained for 1–3 d before recording. Patches used for *G–V* relations contained larger numbers of channels and were typically from oocytes maintained for 3–7 d. Currents typically were digitized at 10–50 kHz. Macroscopic records were filtered at 5 kHz (Bessel low-pass filter; −3 dB) during digitization. Single-channel records were filtered at 10 kHz (Bessel low-pass filter; −3 dB).

During seal formation the oocytes were bathed either in ND-96 or a frog Ringer's solution [containing (in mM) 115 NaCl, 2.5 KCl, 1.8 $CaCl_2$, and 10 HEPES, pH 7.4]. For inside-out patches the patches were excised and moved quickly into a flowing 0 Ca^{2+} solution. The pipette extracellular solution was (in mM) 140 potassium methanesulfonate, 20 KOH, 10 HEPES, and 2 $MgCl_2$, pH 7.0. Test solutions bathing the cytoplasmic face of the patch membrane contained (in mM) 140 potassium methanesulfonate, 20 KOH, 10 HEPES, pH 7.0, and one of the following: 5 mM EGTA (for nominally 0 Ca^{2+} and 1 μM Ca^{2+} solutions), 5 mM HEDTA (for 4 and 10 μM Ca^{2+} solutions, or no added Ca^{2+} buffer (for 60, 100, and 300 μM and 10 mM Ca^{2+} solutions). The methanesulfonate solutions were calibrated to be identical to a set of chloride-containing solutions, with free Ca^{2+} determined from a computer program (EGTAETC; E. McCleskey, Vollum Institute, Portland, OR). To accomplish this, we obtained the desired free Ca^{2+} by titrating the solution with calcium methanesulfonate until the electrode measurement of the methanesulfonate-based solution matched that of a chloride-based solution. The local perfusion of membrane patches was as described previously (Solaro and Lingle, 1992; Solaro et al., 1997).

Voltage commands and the acquisition of currents were accomplished with pClamp 7.0 for Windows (Axon Instruments, Foster City, CA). Currents were converted to conductances by using the measurement capabilities of the ClampFit program. For noninactivating currents the conductances were determined both from tail currents and from the peak current at the activation potential. Both estimates typically agreed within 5 mV. Ensemble averages were generated with custom software. Either null traces or traces obtained in 0 Ca^{2+} were used to generate an idealized leakage trace in the absence of channel openings. Then the idealized record was subtracted from records with channel openings before the detection and idealization of channel activity, using a 50% threshold detection procedure.

G–V curves for noninactivating variants were generated from both peak currents and tail currents with no significant difference in resulting fit values. *G–V* curves for inactivating variants were constructed from peak currents alone. Current values were measured by ClampFit (Axon Instruments), converted to conductances, and then fit with a nonlinear least-squares fitting program. Normalized *G–V* curves were fit with a Boltzmann equation with the form $G(V) = \{1 + \exp[-(V - V_{0.5})]/k\}^{-1}$. *G–V* curves in Figure 8 display the mean and SEM of the values at a given voltage for a set of patches. Because of variability in the *G–V* curves from individual patches, this flattens the *G–V* curve for the populations. Therefore, values for the means of each set of individual *G–V* curves for each patch are provided also.

The onset and recovery from blockade by CTX were fit as described previously (Saito et al., 1997) assuming a simple, first-order bimolecular blocking reaction involving two parameters: *f*, the forward rate of block (in units of M/sec) and *b*, the unblocking rate in seconds. The K_D was calculated from *b*/*f*.

Experiments were done at room temperature (21–24°C). All salts and

chemicals were obtained from Sigma-Aldrich (St. Louis, MO). Trypsin was applied at a concentration of ~0.25 mg/ml.

Removal of inactivation by trypsin. Predictions for the relationship between the apparent inactivation time constant (τ_i) and the fraction of total BK current that is noninactivating current (f_{ss}) were determined on the basis of the following assumptions (Ding et al., 1998). (1) Channels can have 0–4 inactivation domains. All channels in the population start with some average number, n, of inactivation domains per channel. (2) For the total BK channel population the number of inactivation domains per channel follows a binomial distribution. (3) A single inactivation domain is sufficient to produce inactivation, and each inactivation domain acts independently to produce channel inactivation, with the microscopic rate of inactivation of one inactivation domain being k_f (see MacKinnon et al., 1993; Ding et al., 1998). The value of f_{ss} allows for the use of the binomial distribution to calculate the fraction of channels of other stoichiometries. Then, for a given f_{ss}, a predicted macroscopic τ_i can be predicted for the population of channels. Specifically, to determine the predicted τ_i for a set of channels, we determined the contribution of channels of each stoichiometry from $I_m(t) = A_m \cdot \exp(-m \cdot k_f \cdot t)$, where $m = 0–4$ (the number of inactivation domains per channel) and A_m is the fraction of channels containing m inactivation domains. For the set of channels:

$$I(t) = \sum_{m=0.4} I_m(t).$$

The resulting $I(t)$ then was fit with a single exponential function to obtain the predicted τ_i for a given f_{ss}. Although the inactivation time course for a population of channels with different numbers of inactivation domains should exhibit multiple exponential components, in practice the predicted components are difficult to distinguish even with simulated currents. The solid lines in Figure 4 were determined from this procedure with the additional assumption that, for the cases of $n = 3.2$ and 3.6, the initial f_{ss} before the initiation of the digestion was indistinguishable from 0.

RESULTS

Identification of a new BK β-subunit that confers inactivation on BK channels

In a search for novel genes that might contribute to the BK β-subunit family, a gene database search was performed and a human EST was identified that shares partial homology with previously described BK β-subunits from smooth muscle (β1, Knaus et al., 1994a,b) and quail (β2, Oberst et al., 1997) (Fig. 1). A cDNA clone containing the full-length coding region of human β3 (hβ3) was obtained from a human lung neuroendocrine tumor source (Genome Systems, St. Louis, MO). Subsequently, a rat homolog (rβ3) of hβ3 was isolated from a RINm5F cDNA library. The deduced amino acid sequences of both human and rat β3 contain 235 residues that are identical except for 10 amino acids. There are 43% identities and 63% similarities between hβ1 and human hβ3. At the N terminal β3 has no apparent signal peptide, and a hydrophilicity plot shows that it has two hydrophobic regions toward the N and C terminals, which appear to correspond to the proposed transmembrane segments for the β1 subunit (Knaus et al., 1994a) (Fig. 1*B*). There are three potential N-glycosylation sites located between the two hydrophobic regions of β3. The predicted topology of β3 is similar to β1, having two transmembrane segments with both N and C terminals inside the cell and a large extracellular loop that has several N-glycosylation sites. β3 shares with β1 and β2 the presence of four conserved cysteines thought to contribute to the formation of disulfide bridges in the extracellular loop of the subunit.

The expression pattern of β3 in rat and human tissues

Northern blot analysis shows that hβ3 is highly expressed in human kidney, heart, and brain. In kidney and heart two major mRNA products, 1.6 and 2.9 kb, were observed, whereas in brain only a 2.9 kb product was detected (Fig. 2*B*). Low-level expression of hβ3 mRNA products also was detected in human lung, small intestine, spleen, and colon. The relative expression level of β3 in rat tissues differed somewhat from human tissues. As in human tissue, β3 was abundant in brain and heart. However, β3 was expressed more strongly in rat lung and less so in rat kidney, in comparison to human tissue.

We also explicitly tested for the presence of β3 message in tissues known to express inactivating BK channels (Solaro and Lingle, 1992; Li et al., 1999). PCR reactions using substrate cDNA that was reverse-transcribed for rat adrenal and pancreatic tissue generated a single band of the expected size. DNA sequence analysis confirmed that the product in rat adrenals and pancreas is identical to rβ3 (data not shown).

Coexpression of human or rat β3 with *mSlo* α-subunits confers inactivation on BK channels

Expression of either the human or rat β3 subunits with *Slo* α-subunits in *Xenopus* oocytes results in BK-type channels that exhibit rapid inactivation after depolarizing voltage steps in the presence of constant submembrane Ca^{2+} (Fig. 3*A*). Channels exhibited the characteristic large single-channel conductance (~250–260 pS in symmetrical K^+). Ensembles of channel openings arising from the coexpression of the *Slo* and β3 constructs exhibited an apparent inactivation time constant (τ_i) of ~25 msec at +100 mV and 10 μM Ca^{2+}. Figure 3*B* plots ensemble current averages for the patch shown in *A* for 0, 1, 4, and 10 μM Ca^{2+}. As Ca^{2+} is increased, the apparent τ_i becomes faster. Patches with a larger number of channels exhibited similar inactivation behavior (Fig. 3*C* for *Slo* with hβ3). Figure 3*D* displays normalized currents activated at different command potentials but with 10 μM Ca^{2+}. Stronger membrane depolarization increases the apparent τ_i. Figure 3*E* plots the measured τ_i as a function of Ca^{2+} and voltage for currents generated by channels in patches from oocytes injected with *Slo* and human β3. The onset of inactivation appears to reach both a Ca^{2+} and voltage-independent limiting rate, as has been observed for native BK_i channels in chromaffin cells and RIN cells. Estimates of τ_i from ensembles of detected channel openings were indistinguishable from those shown in Figure 3*E* (data not shown). These properties of τ_i closely mirror the behavior of BK_i channels in RIN and chromaffin cells.

Inactivation properties of *Slo*β3 channels share key similarities with native BK_i channels found in RIN and chromaffin cells

We also wished to determine whether other properties of currents arising from *Slo*β3 subunits are consistent with the known properties of BK_i channels in RIN and chromaffin cells.

Inactivation of BK_i channels in native cells involves multiple trypsin-sensitive inactivation domains (Ding et al., 1998). To examine this possibility, we applied trypsin (0.5 mg/ml) for 3–5 sec periods to inside-out patches, and current averages were generated from channels activated between trypsin applications. In Figure 4*A*, trypsin was applied to a patch containing a single inactivating channel. Inactivation was removed gradually by trypsin and eventually was abolished completely. Ensemble averages from patches with one or a small number of channels indicated that trypsin slowed τ_i, although stochastic fluctuations resulted in large variation in such estimates. When patches with larger numbers of channels were used ($n = 4$ patches), trypsin clearly resulted in the gradual removal of inactivation, in a manner consistent with the inactivation of *Slo*β3 channels arising from multiple independent cytosolic inactivation domains per channel

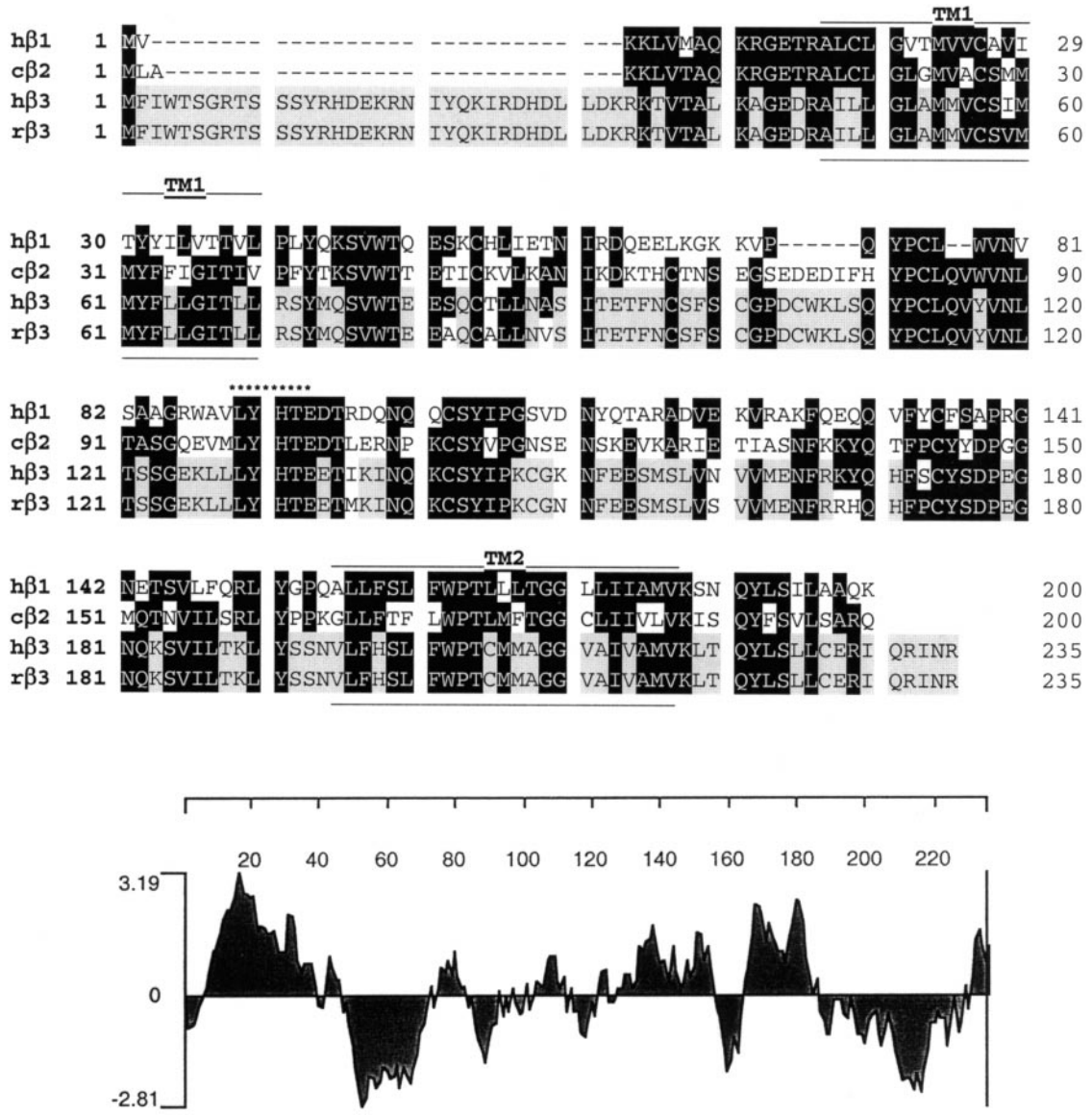

Figure 1. A family of β-subunits for the *Slo* Ca^{2+}-dependent voltage-gated K^+ channel. *Top*, Amino acid alignment of human β1 (*hβ1*), quail β2 (*cβ2*), human β3 (*hβ3*), and rat β3(*rβ3*) subunits. *Darkly shaded* residues are those with identity to aligned residues in at least one other β-subunit family member. *Lightly shaded* residues are those in which rat and human β3 subunits show identity. The two predicted transmembrane segments, *TM1* and *TM2* (Knaus et al., 1994a), are marked with *lines* both *above* and *below*. Residues proposed to be involved in the CTX binding of hβ1 (amino acids 90–94; Hanner et al., 1997) are marked with a *row* of *asterisks*. *Bottom*, Hydrophilicity plot (Kyte–Doolittle algorithm) of hβ3 with a window of nine amino acids.

(Fig. 4*B*). For a given number of inactivation domains per channel, τ_i is predicted to change in accordance with the fraction of current that is noninactivating (see Materials and Methods) (MacKinnon et al., 1993). Such a relationship is plotted for one patch in Figure 4*C*, suggesting that the inactivation of *Slo*β3 currents is consistent with four independent inactivation domains. As in previous work with native BK_i channels (Ding et al., 1998) and earlier work with *Shaker*B K^+ channels (Gomez-Lagunas and Armstrong, 1995), with >50% removal of inactivation the estimates of prolongation are vulnerable to additional slow components of inactivation, resulting in deviation from the predicted relationships. The results in Figure 4 support the idea that multiple independently acting inactivation domains participate in the *Slo*β3 inactivation process. The results also suggest a stoichiometry of four inactivation domains per channel. However, because the experimentally determined relationship between the fractional prolongation of τ_i and the fraction of noninactivating current (f_{ss}) is quite sensitive to rather small variability in the measured estimates of the apparent τ_i before the removal of inactivation, we feel that any conclusion concerning the stoichiometry of inactivation is only tentative at present.

Inactivation of native BK_i channels also exhibits one feature that distinguishes it from inactivation of the *Shaker* family of voltage-dependent K^+ channels (Choi et al., 1991) and from inactivation of BK channels observed in hippocampal neurons (Hicks and Marrion, 1998). Specifically, cytosolic blockers of BK channels do not slow the native BK_i inactivation process (Solaro et al., 1997), indicative that occupancy of a site within the mouth of the ion permeation pathway does not hinder movement of the inactivation domains to their blocking sites. This contrasts with inactivation of BK channels in hippocampal neurons in which TEA and the *Shaker*B ball peptide have been shown to compete

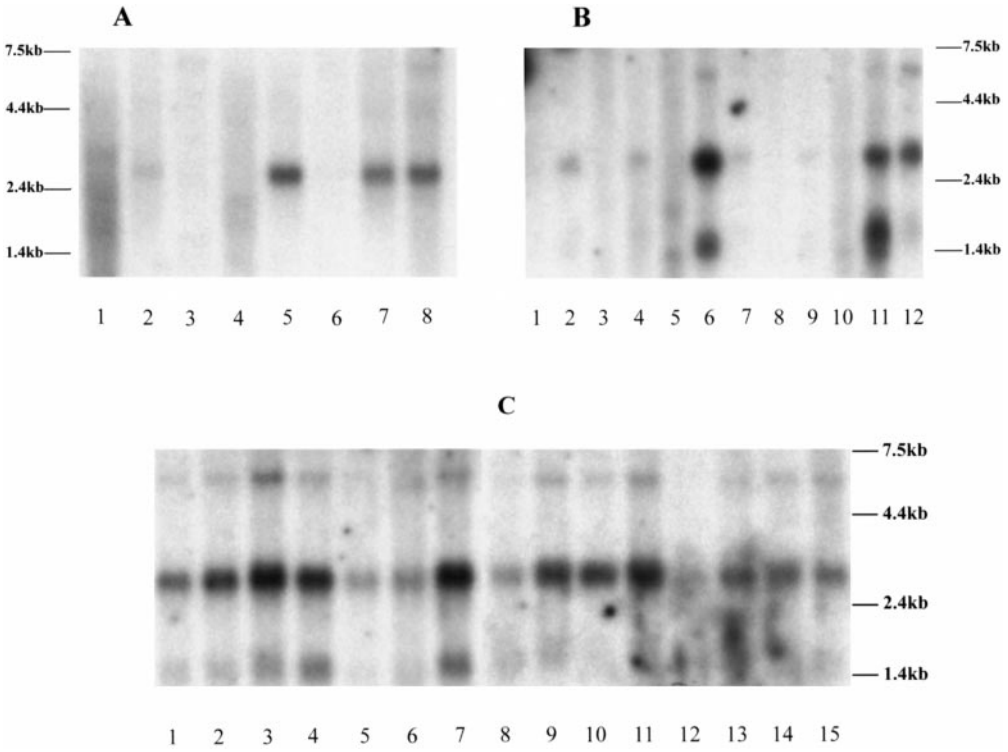

Figure 2. Northern blot analysis of $\beta 3$ subunit distribution. Membranes were probed with radiolabeled $\beta 3$ sequence (h$\beta 3$ for human tissues and r$\beta 3$ for rat tissues). *A*, Rat tissues: *1*, testis; *2*, kidney; *3*, skeletal muscle; *4*, liver; *5*, lung; *6*, spleen; *7*, brain; *8*, heart. *B*, Human tissues: *1*, peripheral blood leukocytes; *2*, lung; *3*, placenta; *4*, small intestine; *5*, liver; *6*, kidney; *7*, spleen; *8*, thymus; *9*, colon; *10*, skeletal muscle; *11*, heart; *12*, brain. *C*, Human brain: *1*, thalamus; *2*, substantia nigra; *3*, whole brain; *4*, hippocampus; *5*, corpus callosum; *6*, caudate nucleus; *7*, amygdala; *8*, putamen; *9*, temporal lobe; *10*, frontal lobe; *11*, occipital pole; *12*, spinal cord; *13*, medulla; *14*, cerebral cortex; *15*, cerebellum.

with the inactivation process (Hicks and Marrion, 1998). We therefore tested whether the rather bulky quaternary ammonium cytosolic blocker of BK channels, the lidocaine derivative QX-314, might hinder the *Slo*$\beta 3$ inactivation process. QX-314 produces a voltage-dependent reduction in BK single-channel current (Oda et al., 1992; Solaro et al., 1997) consistent with a rapid open-channel block mechanism in which QX-314 occupies a site within the ion permeation pathway. In Figure 5*A*, the cytosolic application of 2 mM QX-314 reduced the averaged peak current to ~24% of the control amplitude, having only small effects on τ_i. For a simple model in which QX-314 is proposed to compete with the native inactivation process, a reduction of current to 24% is predicted to produce a 4.17-fold prolongation of τ_i (Choi et al., 1991; Ding et al., 1998). For four patches, 2 mM QX-314 produced a 1.18 ± 0.07-fold prolongation of τ_i. Thus, the effect of QX-314 is inconsistent with a simple competitive scheme, indicative that inactivation conferred by the $\beta 3$ subunit does not involve interaction with the site occupied by QX-314.

The $\beta 3$ subunit confers a reduced sensitivity to CTX

BK_i channels in chromaffin cells (Ding et al., 1998) and RIN cells (Li et al., 1999) exhibit a reduced sensitivity to the scorpion venom, CTX (Ding et al., 1998). Specifically, blockade of BK_i current by CTX exhibits a slower onset and slower recovery than were observed for noninactivating BK current in chromaffin cells (Ding et al., 1998). If incorporation of the $\beta 3$ subunit accounts for the inactivating BK_i phenotype in these cells, it also must confer a reduced sensitivity to CTX. In Figure 6, the sensitivity of *Slo*, *Slo*$\beta 1$, and *Slo*$\beta 3$ channels is compared by using outside-out patches. When 5 mM TEA was applied in the same experiments, complete block and recovery from TEA blockade occurred within the first voltage step after the solution change, an interval of 10–20 sec. Thus, the time course of onset and recovery from block by CTX should reflect the kinetics of the CTX blocking reaction. With *Slo* expression alone, 20 nM CTX produces a relatively complete and rapid block of current. With coexpression of h$\beta 1$ (Fig. 6*B2*), blockade by 20 nM CTX was somewhat less effective at blocking in current, although 100 nM CTX produced an almost complete block. In contrast, an application of 100 nM CTX of duration comparable to that in Figure 6*B2* produced only a slowly developing and incomplete block of the *Slo*h$\beta 3$ current (Fig. 6*B3*). Qualitatively, these results indicate that the $\beta 3$ subunit appears to decrease the amount of block by CTX at a given concentration and to slow the rate of onset of block.

Blockade by CTX for BK channels has been described by a relatively simple bimolecular reaction (MacKinnon and Miller, 1988). With the assumption of this type of reaction, an estimate of the approximate K_D for block by CTX can be obtained from a simultaneous fit of the onset and recovery from block (see Materials and Methods), assuming that the time course of CTX concentration changes is sufficiently rapid relative to the time course of the blocking reactions. This procedure takes advantage not only of information available from the magnitude of blockade produced by one or two concentrations of CTX but also of the rates of the blocking reaction. With the use of this procedure, CTX blocks *Slo* currents with an IC_{50} of 3.5 ± 0.6 nM (mean ± STD; $n = 4$ patches) and blocks *Slo*$\beta 1$ currents with an IC_{50} of 13.9 ± 2.4 nM ($n = 3$). Blockade of *Slo*$\beta 3$ currents was more difficult to assess quantitatively, because washout from CTX blockade was difficult to achieve (Fig. 6*C*). This difficulty in achieving reversibility from CTX block of inactivating BK currents also was observed in chromaffin cells (Ding et al., 1998) and RIN cells (Li et al., 1999). Assuming a simple block model, in which recovery from block is expected to be complete, the example in Figure 6*C* yields an IC_{50} of ~29 nM, although the data are not fully described by this model. With the use of this procedure for three cells with at least partial recovery from block, the IC_{50} was 49.8 ± 26.9 nM. Because of the difficulty in achieving adequate recovery, this value certainly overestimates the sensitivity

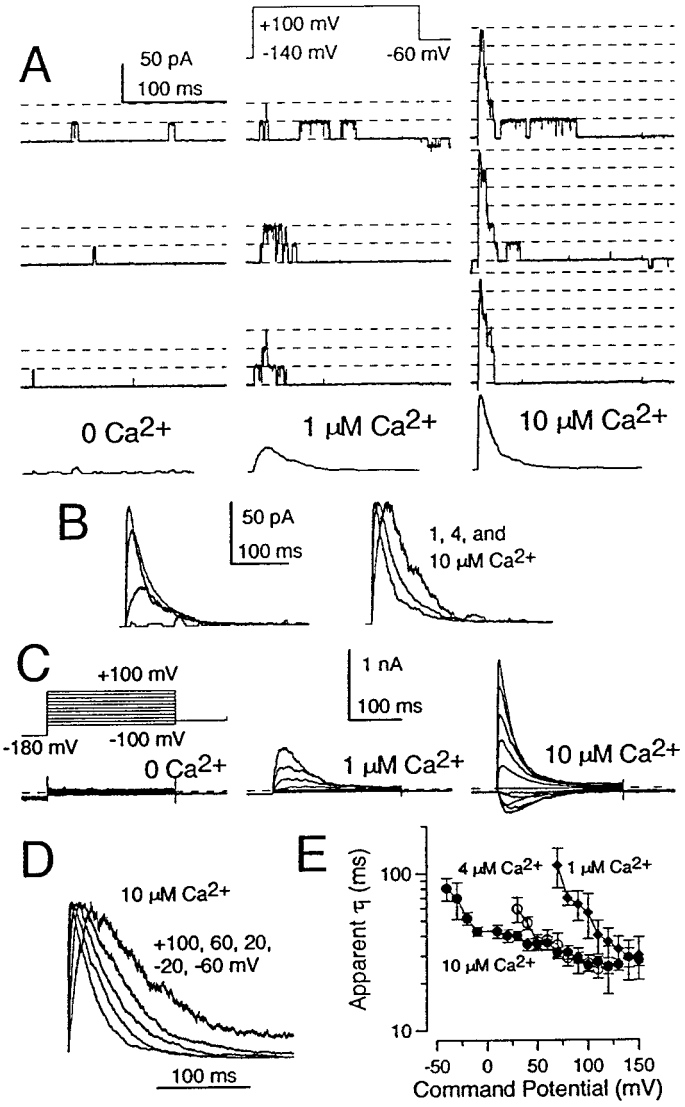

Figure 3. Coexpression of the β3 subunit with the *Slo* α-subunit produces inactivating BK channels. *A*, Traces show channel openings from an inside-out patch from a *Xenopus* oocyte injected with cRNA encoding both rat β3 and mouse *Slo* α-subunits. Channels were activated by voltage steps to +100 mV, after a prepulse to −140 mV to remove inactivation, in the presence of 0, 1, or 10 μM Ca^{2+}. Averages of openings for each condition are shown *below* the traces. *B*, *Left*, Ensemble-averaged currents are overlaid to emphasize differences in the amplitude and time course of current activation and inactivation for 0, 1, 4, and 10 μM Ca^{2+}. *B*, *Right*, Currents obtained at 1, 4, and 10 μM were normalized to the peak current values to allow for a comparison of the time course of inactivation. Increases in Ca^{2+} result in a faster apparent τ_i. *C*, Traces show macroscopic currents recorded from excised inside-out patches, with a larger number of channels resulting from the hβ3 construct coexpressed with *mSlo.* Activation was elicited at potentials from −100 through +100 mV with 0, 1, and 10 μM Ca^{2+}. *D*, *Slo*hβ3 currents activated with 10 μM Ca^{2+} at the indicated voltages were normalized to the same amplitude to show that the apparent τ_i becomes faster with increased depolarization. *E*, The τ_i is plotted as a function of command potential for 1, 4, and 10 μM Ca^{2+}. With sufficient depolarization a similar limiting τ_i of ~25–30 msec is achieved for each [Ca^{2+}].

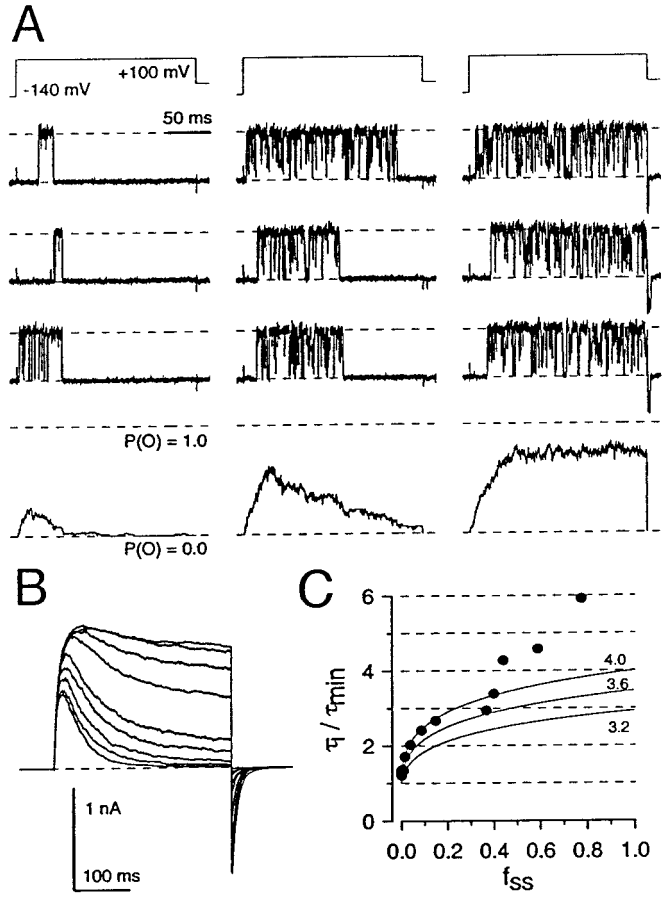

Figure 4. Selective digestion of the inactivation mechanism by trypsin applied to the cytosolic membrane face. *A*, Trypsin (0.5 mg/ml) was applied briefly to a patch containing one BK_i channel resulting from the expression of hβ3 with *mSlo* α-subunits. The cytosolic face of the patch was bathed with 10 μM Ca^{2+}. The *left column* shows traces before trypsin exposure, the *middle column* shows traces after partial trypsin digestion, and the *right column* shows traces after removal of inactivation. Averages expressed as channel open probability (P_O) from each set of sweeps are shown *below* the individual traces. *B*, Ensemble currents from a patch with a larger number of channels are displayed. Channels were activated with 10 μM Ca^{2+}, with voltage steps to +100 mV. Trypsin was applied for 3–5 sec between the generation of each ensemble. As inactivation is removed, there is also a slowing in the apparent τ_i. *C*, The fractional prolongation of τ_i is plotted as a function of the fraction of peak current that does not inactivate by the end of each voltage step. When a limiting τ_i of 28 msec is used, the experimental points closely follow the predictions for a population of channels, each of which initially contained four inactivation domains per channel.

of the *Slo*β3 currents to CTX. The difficulty in obtaining adequate recovery from CTX block of the *Slo*β3 construct may indicate that a simple block scheme may not be fully adequate to describe the blocking mechanism. However, qualitatively, the slower onset of block and weaker blocking effect of CTX on the *Slo*β3 currents relative to *Slo* alone or *Slo*β1 are consistent with the weaker effects of CTX on BK_i currents in RIN and chromaffin cells (Ding et al., 1998). This suggests that the β3 subunit may account for the reduced CTX sensitivity of BK_i channels in these cells.

Two other studies also have reported the existence of BK channels with reduced sensitivity to CTX, but these other channels were noninactivating in nature. First, some BK-type channels studied in bilayers appear to lack sensitivity to CTX (Reinhart et al., 1989). Second, BK channels in peptide-secreting terminals of the posterior pituitary are CTX-resistant (Bielefeldt et al., 1992). Because these other CTX-resistant BK channels are noninactivating, it raises the possibility that additional, unidentified β-subunits may contribute to the properties of these other channels.

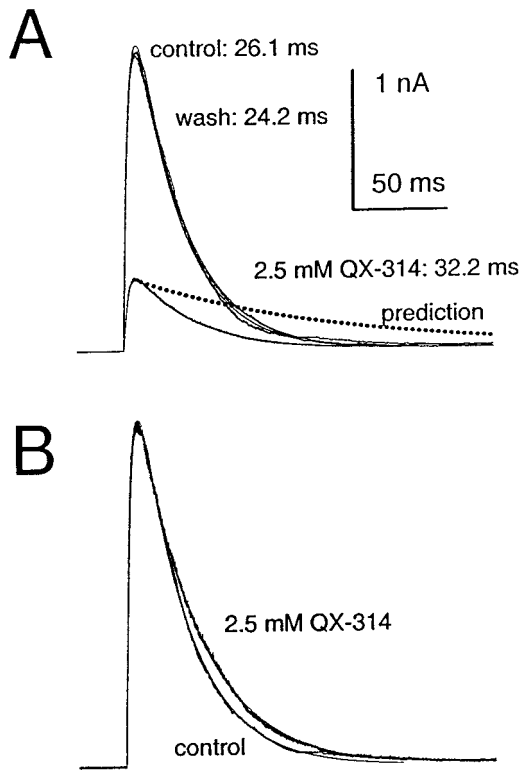

Figure 5. A cytosolic blocker does not slow the inactivation of *Slo*hβ3 currents. *A*, Ensemble current averages obtained before, during, and after the application of 2 mM QX-314 to the cytosolic face of an inside-out patch expressing *Slo*hβ3 channels are plotted. Peak current was reduced to ~24% by QX-314. A simple competitive interaction between QX-314 and movement of the inactivation domain to its blocking site predicts an ~4.17-fold prolongation in current decay, indicated by the *dotted line*. *B*, Normalized currents are plotted to show that QX-314 appears to produce a slight prolongation of current decay. However, the magnitude of the prolongation is inconsistent with that expected for a simple competitive interaction with the inactivation domain and site occupied by QX-314.

The β3 N terminal is necessary and sufficient for inactivation

The additional N-terminal sequence of the β3 peptide suggested that this region was responsible for the inactivation behavior. To address this issue, we created a construct [β3(Δ1–33)] lacking the first 33 amino acids of the β3 sequence. Expression of β3(Δ1–33) with *Slo* completely abolished any rapid inactivation of current (Fig. 7*A*). To verify that the β3(Δ1–33) subunit actually was expressed and associated with *Slo* subunits, we examined the IC_{50} for blockade of *Slo*β3(Δ1–33) by CTX and found it to be 44.5 ± 16.9 nM (n = 3) (see Fig. 6*D*), comparable to results with the intact β3 subunit but distinct from *Slo* alone. Thus, removal of the N terminal from the β3 subunit abolishes inactivation but maintains a change in CTX sensitivity similar to that produced by the intact β3 subunit.

To assess further the role of the β3 N terminal, we used amino acids 1–43 of the β3 subunit to replace the N-terminal 1–12 amino acids of the β1 subunit [hβ3(1–43/hβ1)]. As shown in Figure 7*B*, this addition of the β3 N terminal to the β1 subunit was sufficient to confer inactivation behavior on the β1 subunit. The apparent τ_i for this construct was indistinguishable from that of β3 (data not shown).

The β3 subunit shifts gating of *Slo* subunits

A major functional role of the previously described β1 and β2 subunits is to produce a shift in activation by Ca^{2+} to more negative membrane potentials (McManus et al., 1995; Dworetzky et al., 1996; Wallner et al., 1996; Saito et al., 1997; Ramanathan et al., 1999). Thus, smooth muscle BK channels or other BK channels containing a β1 subunit can be activated by elevations of submembrane Ca^{2+} even at membrane potentials near rest. In contrast, other BK channels in native cells appear to exhibit sensitivities to Ca^{2+} more similar to the *Slo* α-subunit in the absence of any β-subunit (McManus, 1991; Saito et al., 1997).

Given the important role of the β1 subunit in the regulation of gating of the α-subunit, we examined the activation of current by 10 μM Ca^{2+} at various voltages for six different constructs: *Slo* alone, *Slo*hβ3, *Slo*(Δ1–33)β3, *Slo*[β3(1–43)]β1, *Slo*hβ1, and *Slo*rβ3. For constructs that exhibited inactivation (*Slo*hβ3 and *Slo*[β3(1–43)]β1), peak currents were used to generate conductance–voltage (G–V) curves. We expect that estimates of G–V curves for inactivating currents that use the peak current will reduce the steepness of the apparent voltage dependence, thereby producing a somewhat more positive estimate of the $V_{0.5}$. However, the threshold for current activation should be similar with inactivation intact or removed. For the other constructs the G–V curves were generated from both peak and tail currents, with only small differences in the results. Figure 8 plots normalized G–V curves for four constructs. Clearly, both the β1 and β3 subunits result in a substantial shift in the voltage range over which the channel effectively gates with 10 μM Ca^{2+}.

DISCUSSION

The present results demonstrate that the coassembly of *Slo* α-subunits with the β3 subunit is responsible for expression of inactivating BK channels in RIN and chromaffin cells. Furthermore, the presence of the β3 subunit in a number of other tissues, including brain, suggests a more general role of inactivating BK channels than previously realized. The existence of native BK channels with phenotypes unaccounted for by the known β-subunits and known *Slo* splice variants suggests that additional accessory subunits may remain to be identified. For example, the inactivation of hippocampal BK channels (Hicks and Marrion, 1998) cannot be accounted for by the *Slo* splice variants and β-subunits so far described. Similarly, CTX-resistant, but noninactivating, BK channels found in brain (Reinhart et al., 1989; Bielefeldt et al., 1992) would appear to require components other than those so far described. If so, the tissue-specific expression of β-subunits might help to explain the large phenotypic diversity among native BK channels (McManus, 1991).

Our results indicate that the β3 subunit is present in a number of both neuronal and non-neuronal tissues. Although the inactivation of BK-type channels has been observed in a number of cell types [*Drosophila* muscle, Salkoff (1983); chromaffin cells, Solaro and Lingle (1992); RIN cells, Li et al. (1999); hippocampal neurons, Ikemoto et al. (1989) and Hicks and Marrion (1998); skeletal muscle, Pallotta (1985); frog hair cells, Armstrong and Roberts (1999)], it is unclear to what extent the β3 subunit plays a role in many of these cases.

In chromaffin cells and RIN cells the apparent τ_i of inactivation reaches a relatively voltage-independent and Ca^{2+}-independent value at more positive voltages and more elevated Ca^{2+}. In chromaffin cells this value is in the range of 25–40 msec (Solaro and Lingle, 1992; Prakriya et al., 1996). The variability in the chromaffin cells probably arises from the possibility that the BK

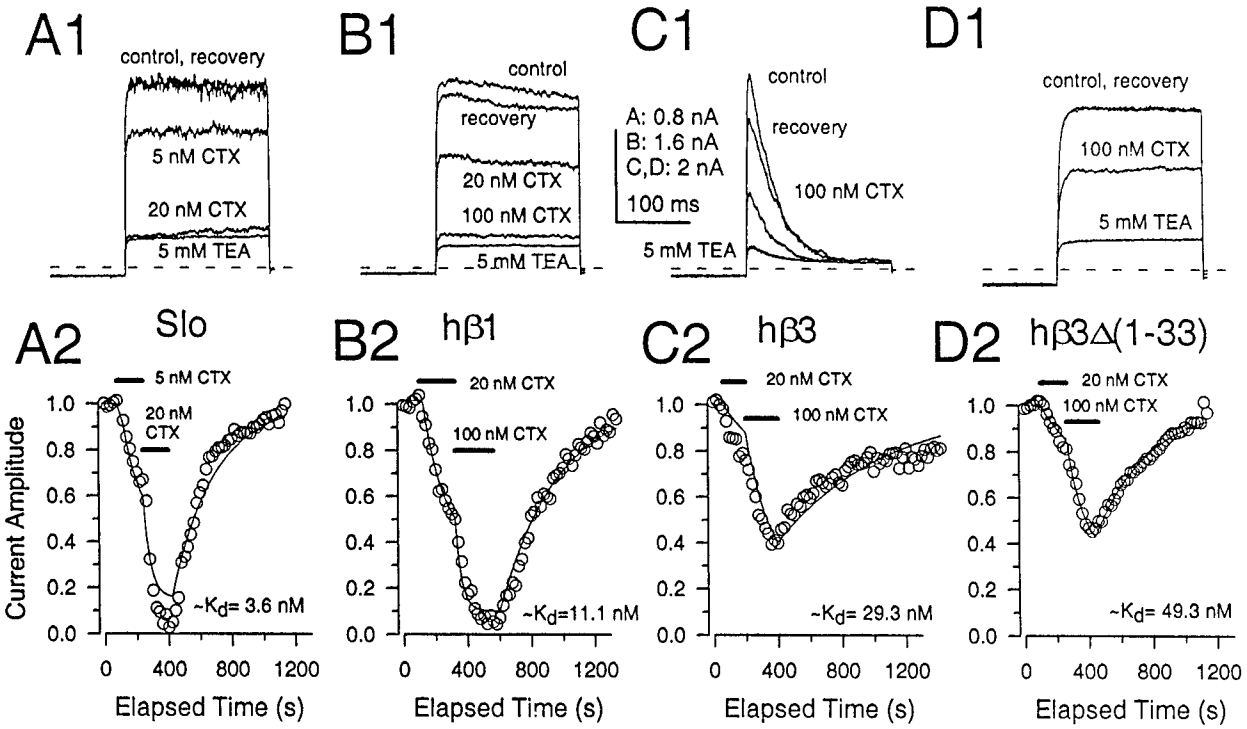

Figure 6. The β3 subunit confers a reduced sensitivity to CTX on the *Slo* subunit. Currents were elicited in outside-out patches with 10 μM pipette Ca^{2+}. Each patch was perfused with the concentrations of CTX indicated by the *horizontal bars*. For each patch 1 or 5 mM TEA also was applied separately to show that the onset and recovery from TEA block were rapid relative to the time course of CTX block. In *A1–D1*, raw currents obtained for control, CTX, and recovery salines are shown for *mSlo* alone (*A*), *mSlo* plus hβ1 (*B*), *mSlo* plus hβ3 (*C*), and *mSlo* plus β3(Δ1–33) (*D*). In *A2–D2*, normalized peak current amplitudes from the patches shown *above* are plotted as a function of elapsed experimental time. The *lines* indicate the optimal fit to a first-order blocking reaction (see Materials and Methods) in which the forward rate of block (*f*, M/sec) and the unblocking rate (*b*, per sec) are the only free parameters. The K_D values calculated from the fit rates are given on the graph, with mean values given in Results.

channels may, on average, contain less than a full complement of four inactivation domains per channel (Ding et al., 1998). In fact, an implication of this latter study was that τ_i for channels containing four inactivation domains should approach ~25–28 msec. This is identical with the limiting τ_i observed here. In contrast, in hippocampus (Hicks and Marrion, 1998) and skeletal muscle (Pallotta, 1985) the inactivation of BK channels is markedly slower (τ_i approximately hundreds of milliseconds). In frog hair cells (Armstrong and Roberts, 1999) the inactivation of a Ca^{2+}-dependent K^+ current is faster (τ_i ~3 msec). Thus, the properties of the apparent τ_i observed for the *Slo*β3 currents are identical to those of BK_i channels in chromaffin cells but differ from those observed in the other tissues.

The inability of QX-314 to hinder the *Slo*β3 inactivation process is similar to the lack of effect of QX-314 on chromaffin cell (Solaro et al., 1997) and RIN cell (Li et al., 1999) BK_i inactivation. In comparison, tetraethylammonium and the *Shaker* ball peptide cause inactivated BK channels in hippocampal neurons to recover from inactivation (Hicks and Marrion, 1998), suggesting a competition between the inactivation domain and the blockers. This again suggests that the inactivation mechanism in the hippocampal cells differs from that resulting from the action of the β3 subunit. Thus, although the β3 subunit may account for BK inactivation in RIN and chromaffin cells, the molecular basis for inactivation in other tissues remains unknown.

One property of the *Slo*β3 currents does vary somewhat from BK_i currents in chromaffin cells. Specifically, the voltage of half-activation at 10 μM Ca^{2+} for *Slo*β3 channels is approximately −20 to −30 mV. This is negative to that reported for the activation of BK_i currents in native chromaffin cells by 10 μM Ca^{2+}, which was ~3 mV (Prakriya et al., 1996). Although a difference in methodology might account for these differences, two other factors may contribute to this difference. First, the stoichiometry of the assembly of β- and α-subunits may influence the gating range of native BK channels. Second, there is evidence that the ability of β-subunits to influence the gating range depends on the identity of the α-subunit splice variant (Ramanathan et al., 1999). Either or both of these factors may contribute to differences in the gating range between native BK channels in chromaffin cells and channels arising from the coexpression of β3 and α-subunits. The possibility that <4 β-subunits may be associated with each BK channel in chromaffin cells is consistent with the observation that, on average, BK_i channels contain only two to three inactivation domains per channel (Ding et al., 1998). Furthermore, chromaffin cells express multiple α-subunit splice variants (Saito et al., 1997), one of which may affect the ability of an associated β-subunit to shift gating (Ramanathan et al., 1999). A complete answer to this issue will require a determination of the exact molecular composition(s) of BK channels in chromaffin cells.

The role of β-subunits in defining CTX sensitivity

Despite the general acceptance of CTX as a blocker of BK channels, there is little detailed information about the effective IC_{50} values for block in native tissues. This certainly stems in part from the challenges associated with the slow dissociation of CTX. Some studies also have described CTX-resistant BK channels (Reinhart et al., 1989; Bielefeldt et al., 1992). Our previous studies on chromaffin and RIN cells (Ding et al., 1998; Li et al.,

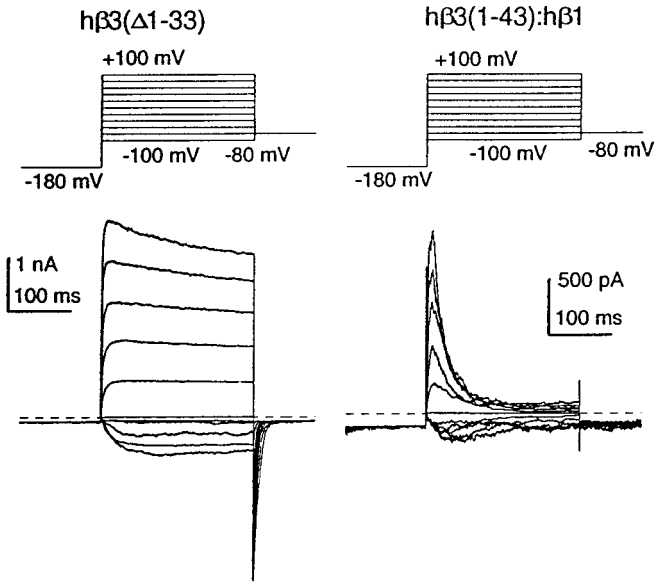

Figure 7. The N terminal of the β3 subunit is necessary and sufficient for inactivation. *A*, *Left*, Currents are shown resulting from the coexpression of *mSlo* with the hβ3(Δ1–33) construct in which 33 amino acids were removed from the hβ3 N terminal. *A*, *Right*, Shown are currents resulting from the coexpression of *mSlo* with the hβ3(1–43):hβ1 construct in which the initial 43 amino acids of hβ3 replaced the first 12 amino acids at the N terminal of hβ1. In both cases the currents were activated by the indicated voltage steps with 10 μM Ca^{2+}. No inactivation is observed with hβ3(Δ1–33), whereas inactivation is observed with hβ3(1–43):hβ1.

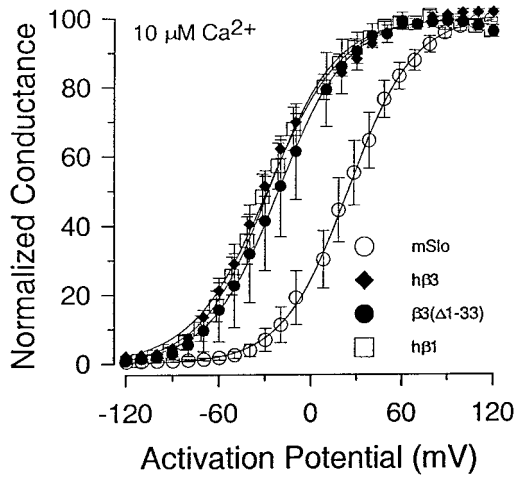

Figure 8. The β3 subunit shifts gating of the *mSlo* α-subunit. Normalized conductance–voltage curves were constructed from each of the indicated constructs by using 10 μM Ca^{2+} to activate the currents. *G–V* curves from individual patches were normalized separately and then averaged. This results in a flattening of the *G–V* curve for the averages. The fit values for the $V_{0.5}$ for the grouped data for each construct included the following: for *Slo* alone, 24.5 ± 0.5 mV (± 90% confidence limit of fit value); for *Slo* plus hβ3, −28.5 ± 1.4 mV; for *Slo* plus β3(Δ1–33), −21.4 ± 0.6 mV; and for *Slo* plus hβ1, −28.1 ± 0.9 mV. For comparison, the means of the $V_{0.5}$ values from each individual patch included the following: for *Slo* alone, 25.8 ± 11.8 mV (mean ± STD; $n = 5$); for *Slo* plus hβ3, −32.6 ± 11.5 mV ($n = 11$); for *Slo* plus β3(Δ1–33), −22.2 ± 19.3 mV ($n = 4$); and for *Slo* plus hβ1, −27.2 ± 18.0 mV ($n = 9$). For six patches with the rat β3 coexpressed with *Slo*, the $V_{0.5}$ was −19.5 ± 7.8 mV. For nine patches for the β3(1–43):β1 construct expressed with *Slo*, the $V_{0.5}$ was −55.5 ± 10.2 mV.

1999) demonstrated a reduced CTX sensitivity (IC_{50} ~50–100 nM) for BK_i channels relative to noninactivating BK channels (IC_{50} ~2–4 nM). Although our results with CTX only provide a qualitative comparison of the effect of β-subunits in defining the CTX sensitivity of different *Slo* channels, the similar resistance of the BK_i and *Slo*β3 channels to CTX is consistent with the proposed role of β3 subunits in the formation of BK_i channels. Our results also suggest that there are differences between the β1 and β3 subunits in determining CTX sensitivity. Residues on the β1 subunit responsible for influencing the affinity of CTX for the *Slo*β complex have been determined (Hanner et al., 1998). Surprisingly, the residues proposed to account for CTX interaction with the β1 subunit are identical in the β3 subunit. Thus, other differences between the β1 and β3 subunits must account for the differences in CTX sensitivity.

The mechanism of BK_i inactivation

The present results indicate unambiguously that the N-terminal domain of the β3 subunit is responsible for the inactivation of the *Slo*β3 channels. Although inactivation of BK_i channels shares some features in common with N-terminal-mediated inactivation (Solaro et al., 1997), there are also clear differences. Unlike inactivation mediated by the N terminal of the *Shaker*B α-subunit (Choi et al., 1991; Demo and Yellen, 1991), inactivation mediated by the tethered β3 N-terminal domain involves a binding site not influenced by occupancy of the ion permeation pathway by QX-314. Thus, the β3 N-terminal domain appears to block the BK channel at a position probably not homologous with the *Shaker* pore site acted on by the *Shaker*B N-terminal structures.

During the revision of this manuscript, a paper describing the identical human β-subunit appeared (termed β2 in Wallner et al., 1999). Our results share a number of observations with this other study but differ on some interesting points. First, in the other work, Northern blots did not reveal the β3 subunit in adrenal tissue. In contrast, our results support the view that the β3 subunit can account specifically for BK channel inactivation in RIN cells and chromaffin cells. Specifically, we showed by PCR that the β3 subunit is found in pancreatic and chromaffin cell RNA and that the β3 subunit is present in a RIN cell library. It is possible that low message levels may result in the difficulty of detecting the β3 subunits by Northern blots. Second, our results indicate that QX-314 does not compete with the native inactivation process mediated by the β3 subunit, similar to the properties of BK_i channels in native cells (Solaro et al., 1997). However, Wallner et al. (1999) report that TEA does compete with a free β3 N-terminal ball peptide for blockade of the *Slo* channel. To address this potential discrepancy, we therefore have examined the ability of QX-314 to compete with a 26-amino-acid β3 N-terminal peptide and find that QX-314 does hinder the ability of the free N-terminal peptide to block *Slo* channels (C. Lingle, unpublished observations). Thus, the two sets of results are not inconsistent but raise the interesting possibility that the blocking site reached by isolated N-terminal peptides is not identical to that reached by the tethered β3 N terminal. The availability of the key structures required for inactivation will now allow the issue of the binding site of the inactivation domain to be addressed.

REFERENCES

Adelman JP, Shen K-Z, Kavanaugh MP, Warren RA, Wu Y-N, Lagrutta A, Bond CT, North RA (1992) Calcium-activated potassium channels expressed from complementary DNAs. Neuron 9:209–216.

Armstrong CE, Roberts WM (1999) A very rapidly inactivating calcium-

dependent potassium current in frog saccular hair cells. Biophys J 76:A74.
Atkinson NS, Robertson GA, Ganetsky B (1991) A component of calcium-activated potassium channels encoded by the *Drosophila slo* locus. Science 253:551–553.
Bielefeldt K, Rotter KL, Jackson MB (1992) Three potassium channels in rat posterior pituitary nerve terminals. J Physiol (Lond) 458:41–67.
Butler A, Tsunoda S, McCobb DP, Wei A, Salkoff L (1993) *mSlo*, a complex mouse gene encoding "maxi" calcium-activated potassium channels. Science 261:221–224.
Choi KL, Aldrich RW, Yellen G (1991) Tetraethylammonium blockade distinguishes two inactivation mechanisms in voltage-activated K^+ channels. Proc Natl Acad Sci USA 88:5092–5095.
Demo SD, Yellen G (1991) The inactivation gate of the *Shaker* K^+ channel behaves like an open-channel blocker. Neuron 7:743–753.
Ding JP, Li ZW, Lingle CJ (1998) Inactivating BK channels in rat chromaffin cells may arise from heteromultimeric assembly of distinct inactivation-competent and noninactivating subunits. Biophys J 74:268–289.
Dworetzky SI, Boissard CG, Lum-Ragan JT, McKay MC, Post-Munson DJ, Trojnacki JT, Chang C-P, Gribkoff VK (1996) Phenotypic alteration of a human BK (*hslo*) channel by *hslo*β subunit coexpression: changes in blocker sensitivity, activation/relaxation and inactivation kinetics, and protein kinase A modulation. J Neurosci 16:4543–4550.
Gomez-Lagunas F, Armstrong CM (1995) Inactivation in *Shaker*B K^+ channels: a test for the number of inactivating particles on each channel. Biophys J 68:89–95.
Hamill OP, Marty A, Neher E, Sakmann B, Sigworth FJ (1981) Improved patch-clamp techniques for high-resolution current recording from cells and cell-free membrane patches. Pflügers Arch 391:85–100.
Hanner M, Schmalhofer WA, Munujos P, Knaus H-G, Kaczorowski GJ, Garcia ML (1997) The β-subunit of the high-conductance calcium-activated potassium channel contributes to the high-affinity receptor for charybdotoxin. Proc Natl Acad Sci USA 94:2853–2858.
Hanner M, Vianna-Jorge R, Kamassah A, Schmalhofer WA, Knaus HG, Kaczorowski GJ, Garcia ML (1998) The β-subunit of the high conductance calcium-activated potassium channel. Identification of residues involved in charybdotoxin binding. J Biol Chem 273:16289–16296.
Hicks GA, Marrion NV (1998) Ca^{2+}-dependent inactivation or large-conductance Ca^{2+}-activated K^+ (BK) channels in rat hippocampal neurones produced by pore block from an associated particle. J Physiol (Lond) 508:721–734.
Hoshi T, Zagotta WN, Aldrich RW (1990) Biophysical and molecular mechanisms of *Shaker* potassium channel inactivation. Science 250:533–538.
Ikemoto Y, Ono K, Yoshida A, Akaike N (1989) Delayed activation of large-conductance Ca^{2+}-activated K channels in hippocampal neurons of the rat. Biophys J 56:207–212.
Knaus H-G, Folander K, Garcia-Calvo M, Garcia ML, Kaczorowski GJ, Smith M, Swanson R (1994a) Primary sequence and immunological characterization of the β-subunit of the high-conductance Ca^{2+}-activated K^+ channel from smooth muscle. J Biol Chem 269:17274–17278.
Knaus H-G, Garcia-Calvo M, Kaczorowski GJ, Garcia ML (1994b) Subunit composition of the high-conductance calcium-activated potassium channel from smooth muscle, a representative of the *mSlo* and slowpoke family of potassium channels. J Biol Chem 269:3921–3924.
Li ZW, Ding JP, Kalyanaraman V, Lingle CJ (1999) RINm5f cells express inactivating BK channels, while HIT cells express noninactivating BK channels. J Neurophysiol 81:611–624.
MacKinnon R, Miller C (1988) Mechanism of charybdotoxin block of Ca^{2+}-activated K^+ channels. J Gen Physiol 91:335–349.
MacKinnon R, Aldrich RW, Lee AW (1993) Functional stoichiometry of *Shaker* potassium channel inactivation. Science 262:757–759.
McManus OB (1991) Calcium-activated potassium channels: regulation by calcium. J Bioenerg Biomembr 23:537–560.
McManus OB, Helms LMH, Pallanck L, Ganetsky B, Swanson R, Leonard RJ (1995) Functional role of the β-subunit of high-conductance calcium-activated potassium channels. Neuron 14:645–650.
Meera R, Wallner M, Toro L (1999) Molecular determinant of MAXI K_{Ca} channel inactivation. Biophys J 76:A267.
Oberst C, Weiskirchen R, Hartl M, Bister K (1997) Suppression in transformed avian fibroblasts of a gene (CO6) encoding a membrane protein related to mammalian potassium channel regulatory subunits. Oncogene 14:1109–1116.
Oda M, Yoshida A, Ikemoto Y (1992) Blockade by local anesthetics of the single Ca^{2+}-activated K^+ channel in rat hippocampal neurones. Br J Pharmacol 105:63–70.
Pallotta BS (1985) Calcium-activated potassium channels in rat muscle inactivated from a short-duration open state. J Physiol (Lond) 363:501–516.
Prakriya M, Solaro CR, Ding JP, Lingle CJ (1996) $[Ca^{2+}]_i$ elevations detected by BK channels during Ca^{2+} influx and muscarine-mediated release of Ca^{2+} from intracellular stores in rat chromaffin cells. J Neurosci 16:4344–4359.
Ramanathan K, Michael TH, Jiang G-J, Hiel H, Fuchs PA (1999) A molecular mechanism for electrical tuning of cochlear hair cells. Science 283:215–217.
Reinhart PH, Chung S, Levitan IB (1989) A family of calcium-dependent potassium channels from rat brain. Neuron 2:1031–1041.
Saito M, Nelson C, Salkoff L, Lingle CJ (1997) A cysteine-rich domain defined by a novel exon in a *Slo* variant in rat adrenal chromaffin cells and PC12 cells. J Biol Chem 272:11710–11717.
Salkoff L (1983) *Drosophila* mutants reveal two components of fast outward current. Nature 302:249–251.
Shen K-Z, Lagrutta A, Davies NW, Standen NB, Adelman JP, North RA (1994) Tetraethylammonium block of *Slowpoke* calcium-activated potassium channels expressed in *Xenopus* oocytes: evidence for tetrameric channel formation. Pflügers Arch 408:98–111.
Solaro CR, Lingle CJ (1992) Trypsin-sensitive, rapid inactivation of a calcium-activated potassium channel. Science 257:1694–1698.
Solaro CR, Prakriya M, Ding JP, Lingle CJ (1995) Inactivating and non-inactivating Ca^{2+}- and voltage-dependent K^+ current in rat adrenal chromaffin cells. J Neurosci 15:6110–6123.
Solaro CR, Ding JP, Li ZW, Lingle CJ (1997) The cytosolic inactivation domains of BK_i channels do not behave like simple, open-channel blockers. Biophys J 73:819–830.
Tseng-Crank J, Foster CD, Krause JD, Mertz R, Godinot N, DiChiara TJ, Reinhart PH (1994) Cloning, expression, and distribution of functionally distinct Ca^{2+}-activated K^+ channel isoforms from human brain. Neuron 13:1315–1330.
Tucker SJ, Bond CT, Herson P, Pessia M, Adelman JP (1996) Inhibitory interactions between two inward rectifier K^+ channel subunits mediated by the transmembrane domains. J Biol Chem 271:5866–5870.
Wallner M, Meera P, Toro L (1996) Determinant for β-subunit regulation in high-conductance voltage-activated and Ca^{2+}-sensitive K^+ channels: an additional transmembrane region at the N terminus. Proc Natl Acad Sci USA 92:14922–14927.
Wallner M, Meera P, Toro L (1999) Molecular basis of fast inactivation in voltage- and Ca^{2+}-activated K^+ channels: a transmembrane β-subunit homolog. Proc Natl Acad Sci USA 96:4137–4142.
Wei A, Solaro C, Lingle C, Salkoff L (1994) Calcium sensitivity of BK-type K_{Ca} channels determined by a separable domain. Neuron 13:671–681.
Xia X-M, Hirschberg B, Smolik S, Forte M, Adelman JP (1998a) dSlo interacting protein 1, a novel protein that interacts with large-conductance calcium-activated potassium channels. J Neurosci 18:2360–2369.
Xia X-M, Fakler B, Rivard A, Wayman G, Johnson-Pais T, Keen JE, Ishii T, Hirschberg B, Bond CT, Lutsenko S, Maylie J, Adelman JP (1998b) Mechanism of calcium gating in small-conductance calcium-activated potassium channels. Nature 395:503–507.
Xie J, McCobb DP (1998) Control of alternative splicing of potassium channels by stress hormones. Science 280:443–446.